

Influence of Ink Formulation and Drying Parameters on Component Composition during Drying of Catalyst Layers for Polymer Electrolyte Membrane Fuel Cells and Electrolyzers

Nadine Zimmerer,* Philipp Quarz, Ellen Terhorst, Linus Janning, Philip Scharfer, and Wilhelm Schabel

The formulation and production of catalyst coatings significantly impact the porous microstructure and the performance of electrodes in polymer electrolyte membrane (PEM) fuel cells and electrolyzers. The critical step in the microstructure formation is the drying. Experimental studies have shown that the drying changes the solvent composition, affecting particle- and ionomer (self-) interactions, as well as ink properties, which influence the drying-induced stress build-up within the layers. This study provides a theoretical analysis of the drying of binary 1-propanol/water mixtures, and the transfer to the drying of catalyst inks. On the basis of selective drying, considering thermodynamic selectivity and gas-phase kinetics, the accumulation and depletion of solvents during the drying process is described. The influence of different ink formulations (initial solvent compositions) and drying conditions (air temperature, heat transfer coefficient, and air pre-loading) on ink composition during drying is studied. The selectivity is particularly influenced by the air pre-loading, for example, relative humidity, which inhibits the evaporation kinetics of water. Theoretical predictions from the drying simulations are experimentally validated via gravimetric drying curves using different catalyst ink formulations. The results suggest that the catalyst layer drying can be effectively modeled by focusing solely on the evaporation dynamics of the solvent mixture.

However, there are still obstacles hindering the scale-up of the systems, such as the high material costs. The key component of the systems is the catalyst-coated membrane (CCM), a polymer membrane coated with thin porous catalyst layers, where the energy-converting reactions take place. This key component currently accounts for up to 47% of the stack costs, depending on the annual production rate.^[1]

In recent years, extensive research has been carried out in various areas of the CCM production. The state-of-the-art CCM manufacturing process involves mixing a homogeneous catalyst ink, applying and drying the catalyst ink on an inert decal substrate, and transferring the electrode to the proton-conducting membrane by means of a hot-pressing step. Extensive studies have been made on the development and validation of more efficient and platinum-reduced catalysts,^[2] the influence of ink formulation and ink processing on the performance of the systems,^[3–6] the assessment of different coating processes for the catalyst layers,^[4,7–9] including a

comparison of different coating methods, as well as first insights into electrode drying^[4,6,10] and cracking.^[10–15]


The present study focuses analytically and experimentally on drying of the catalyst electrode as a function of ink formulation (solvent ratio) and drying parameters. The drying of catalyst inks, which are composed of several components including platinum on carbon (Pt/C) catalyst, ionomer, and alcohol/water mixtures, is a complex process. Various effects, such as the selectivity of drying of multicomponent mixtures, have a decisive influence on the solvent composition in the layer during the processing.^[6,10,15–17]

The choice of the materials and coating processes in CCM production requires the use of different solvents and solvent mixtures in catalyst inks.^[9,11,14,18] Typical solvent mass fractions are between 80 and 90 wt% in slot die and doctor blade coating and even higher in ink jet printing.^[4,9,19–22] A commonly used binary solvent mixture consists of a mixture of 1-propanol (P) and water (W), which serves as a representative basis for the investigations presented in this study.^[14,23–25]

1. Introduction

Polymer electrolyte membrane (PEM) fuel cells and electrolyzers present a promising opportunity to produce and utilize green hydrogen as a clean energy source in various applications.

N. Zimmerer, P. Quarz, E. Terhorst, L. Janning, P. Scharfer, W. Schabel
Thin Film Technology (TFT)
Karlsruhe Institute of Technology (KIT)
Straße am Forum 7, D-76131 Karlsruhe, Germany
E-mail: nadine.zimmerer@kit.edu

 The ORCID identification number(s) for the author(s) of this article can be found under <https://doi.org/10.1002/ente.202500516>.

© 2025 The Author(s). Energy Technology published by Wiley-VCH GmbH. This is an open access article under the terms of the Creative Commons Attribution License, which permits use, distribution and reproduction in any medium, provided the original work is properly cited.

DOI: 10.1002/ente.202500516

1.1. Selectivity of the Drying of Catalyst Inks

From a thermodynamic approach, 1-propanol/water mixtures form an azeotrope. This means that, depending on the initial solvent composition, 1-propanol or water will evaporate preferentially (selective evaporation). Consequently, during solvent evaporation, the preferred evaporating component is relatively depleting in the remaining liquid while the total solvent amount is also decreasing.^[10,15,17] The solvent composition is changing during the drying process and varies from the initial solvent composition. Solely at the azeotropic composition the solvent mixture is evaporation unselectively.

When investigating the drying behavior and selectivity of catalyst ink formulations, the thermodynamics of the system must not be assumed as the only factor influencing the ink composition in convective drying. The mass transport kinetics of the solvents in the drying air must also be included in the consideration (e.g., diffusion coefficients, partial pressures, and driving evaporation gradients of the components). This shifts the critical concentration for unselective evaporation from the azeotropic composition (AZ) to the arheotropic (AR) composition according to Quarz et al.^[17] The thermodynamic azeotrope of a mixture is a function of temperature. At a constant temperature, a single azeotropic point can be determined. However, when considering the gas kinetics at a constant temperature, multiple arheotropic points (AR) will emerge, influenced by, for example, the driving evaporation gradients.

With 1-propanol fractions lower than the arheotropic composition, 1-propanol evaporates faster, resulting in a depletion of the alcohol. For fractions greater than the arheotropic composition, water evaporation is favored.^[10,11,17] The arheotropic composition depends on the temperature and solvent pre-loading of the drying air (e.g., relative humidity). In previous studies on binary 1-propanol/water mixtures, Quarz et al.^[17] were able to demonstrate experimentally the variation in solvent composition under different drying conditions. Additionally, they experimentally determined the AZ and AR corresponding to the specific drying parameters employed in their study.

The changing ink solvent composition (e.g., resulting in a change in permittivity of the mixture) is influencing the particle–particle as well as the particle–ionomer interactions, along with the ionomer morphology and interaction affinity.^[4,7,10,24–26] The surface tension and density of the solvent mixture are also affected and could therefore influence the capillary pressure during electrode drying.^[27] An impact of these changes on the formation of the microstructure, including the formation of cracks in the layers, is expected and assessed in this study.

1.2. Microstructure and Crack Formation during Drying of the Catalyst Layers

The important step for the microstructure development is the drying of the catalyst ink. When drying thin, particulate layers, the drying process can be divided into different stages. During the first drying period the solvents evaporate on the surface of the coating. As the solvent content is reduced, the wet film thickness decreases and the particles approach each other. The film reaches a concentration-dependent adiabatic wet-bulb temperature due to

the equilibrium between the energy input and the evaporative cooling. This wet-bulb temperature is influenced by the solvents and the solvent composition of the ink, the drying conditions—such as drying air temperature and humidity—and other non-convective heat fluxes.^[10,28–30]

The first drying stage ends when the particles can no longer approach each other, and the film has reached its final thickness and porosity. This moment in time is referred to as “end-of-film shrinkage” (EOFS).^[30] The solvent mass fraction at the theoretical EOFS ($x_{i,EOFS}$) can be determined according to Jaiser et al.^[30] by using Equation (1) including the porosity of the dry layer ε , the density of the solids ρ_{solids} and the density of the solvent mixture $\rho_{solvents}(x_i)$.

$$x_{i,EOFS} = \left(\frac{1 - \varepsilon}{\varepsilon} \frac{\rho_{solids}}{\rho_{solvents}(x_i)} + 1 \right)^{-1} \quad (1)$$

The solvent density is a function of the mass fraction of the mixture components x_i and can change during the drying process. The porosity of the electrode can be determined experimentally using mercury porosimetry or gas adsorption.

After the EOFS, a porous and solvent-filled particle layer is present. Subsequent to the EOFS, the solvent evaporates from the pore network of the electrode, leading to the development of the porous microstructure. Cracking is anticipated once the solvent recedes into the pore structure of the electrode. The capillary pressures and electrode–substrate interactions cause stress to build up within the layer. When these stresses exceed a critical value, crack formation occurs.^[10,28] The capillary pressure is influenced by the surface tension of the solvents and thus the composition of the solvent mixture.^[27,31,32] Additional parameters for crack formation influenced by solvent composition include particle–particle and particle–ionomer interactions, as previously mentioned. These interactions affect the agglomerate sizes and the particle volume fraction of the close packing, thereby influencing the mechanical stability of the drying layer.^[31,32] Therefore, the evolving solvent composition up to and at the EOFS plays a critical role in understanding crack formation within the catalyst layers. Various studies have demonstrated that cracks in the catalyst layer can negatively affect fuel cell performance and, more critically, long-term durability, for example, by the promotion of membrane degradation and by the reduction of in-plane electrical conductivity.^[4,15,20,33,34] Nonetheless, cracks may also enhance the transport of reactants (e.g., oxygen) and reaction products (e.g., water), improving performance during early-stage operation.^[35] Currently ongoing research focuses on the mechanisms of cracking and their impact on performance and lifetime of PEM systems.

2. Modeling of the Solvent Compositions in Catalyst Layers

In order to gain a better understanding of the drying-related changes in ink composition and their potential impact on electrode properties, the drying of a binary solvent mixture of 1-propanol (P) and water (W) is examined. In the first drying phase, up to the end-of-film shrinkage, the liquid-side mass transport resistance is not significant compared to the strongly

gas-side controlled evaporation and is therefore neglected at this point, assuming no significant influence of the ionomer until EOFs. Therefore, for the first drying period, an approximation of the drying behavior only considering the pure solvent mixture is considered sufficient and is later compared to experimental results of drying catalyst layers.

Based on the non-stationary enthalpy and mass balances of the film (pure solvent mixture without ionomer and catalyst particles) and the evaporation kinetics, three differential equations (see Equation 2–4) can be derived to describe the selective drying of the binary solvent mixture. These equations calculate the mass fraction of the component i x_i in the remaining film, the decrease in total solvent mass M and the film temperature T_{film} , during the first drying period as a function of the drying time t . The energy input is provided by a convective heat flux onto the film, while the bottom of the catalyst layer is assumed to be adiabatic as a first approximation.

$$\frac{dH_{\text{film}}}{dt} = \frac{d(M_{\text{film}}c_{p,\text{film}}(T_{\text{film}} - T_0))}{dt} = \dot{Q}_{\text{conv}} - \dot{H}_{\text{evap}} \quad (2)$$

$$\frac{dM}{dt} = -\dot{M} = -(\dot{M}_W + \dot{M}_P) \quad (3)$$

$$\frac{dM_i}{dt} = x_i \frac{dM}{dt} + M \frac{dx_i}{dt} = -\dot{M}_i \quad (4)$$

The non-stationary enthalpy balance comprise of the heat input from the convective drying nozzles \dot{Q}_{conv} and the enthalpy loss due to solvent evaporation \dot{H}_{evap} . Here, M_{film} is the film mass, $c_{p,\text{film}}$ its heat capacity and T_0 the film temperature at the start of the drying. \dot{Q}_{conv} depends on the heat transfer coefficient α , the surface area A and the drying air temperature T_{conv} . \dot{H}_{evap} is determined by the evaporating mass flow rate \dot{M} and the enthalpy for vaporization. \dot{M} is calculated from the individual substance flows \dot{M}_i . The kinetics of mass transfer is described by the approach based on Fick's law, based on low solvent concentrations in substantially large gas-phase volume.^[36] Raoult-Dalton's law is used for the gas liquid equilibrium. Vapor pressures are calculated using the Wagner equation,^[37] providing accurate representation over a wide temperature range. Molar excess enthalpies are integrated using the van Laar model,^[38] which is well-suited for binary non-ideal liquid mixtures. The simulation assumes that the evaporation is governed by both thermodynamics and gas-phase kinetics and that the solvent evaporation mass flow is significantly lower than the convective flow of the drying air. Gas-phase diffusion coefficients are calculated based on the Fuller's equations, which estimates binary diffusion from molecular structure and diffusion volumes.^[39]

For solving the differential equations the initial value problem (IVP) solver from the SciPy library is used. In the final step, the molar flow rates are converted to mass flow rates to facilitate clearer visualization and interpretation of the data.

Firstly, a purely thermodynamic approach and an extended model that incorporates gas kinetics at a constant temperature of 25 °C, as previously mentioned by Quarz et al.^[17] is compared. The analysis is performed assuming isothermal conditions. The temperature of the liquid phase is adopted as reference temperature. **Figure 1** shows the direct comparison of the purely

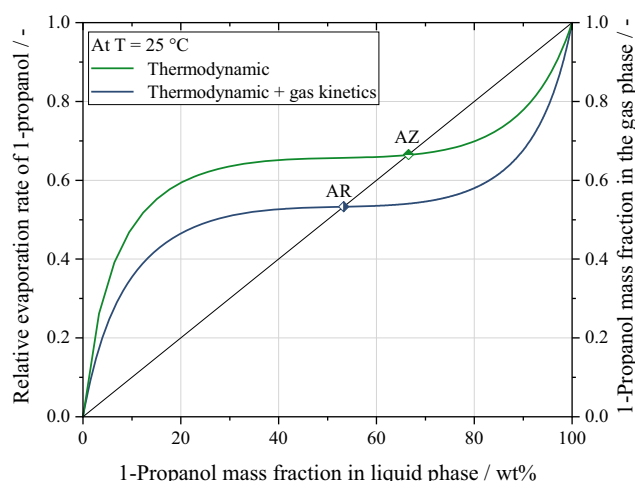


Figure 1. Relative gravimetric evaporation rate of 1-propanol $\dot{M}_P/(\dot{M}_P + \dot{M}_W)$ for thermodynamic and gas kinetics consideration and 1-propanol content in the gas phase y_P for pure thermodynamic consideration as a function of the liquid composition (1-propanol (P) mass fraction x_P) of a binary 1-propanol/water solvent mixture at 25 °C. The sole consideration of the thermodynamics lead to the azeotropic point ($x_{P,AZ} = 66.5$ wt%). Including gas kinetics to the thermodynamic model leads to the azeotropic point ($x_{P,AR} = 53.3$ wt%) (gas temperature 25 °C, dry air).

thermodynamic approach (green), that is, the composition of the liquid phase (x_P) versus the composition of the gas phase (y_P) of the 1-propanol/water mixture (secondary y-axis, McCabe-Thiele diagram). At the AZ the compositions of the liquid and gas phases are identical (Equation (5)) and the mixture is evaporating unselectively.

$$x_{P,AZ} = y_{P,AZ} \quad (5)$$

For the extended drying analysis, gas kinetics are incorporated. The relative (gravimetric) evaporation rate of 1-propanol $\dot{M}_P/(\dot{M}_P + \dot{M}_W)$ over the composition of the liquid phase during drying with dry air is shown in blue (primary y-axis). $\dot{M}_P/(\dot{M}_P + \dot{M}_W)$ can be understood as the composition of the evaporating mass flow and is therefore comparable to the composition in the gas phase. Equal gas and liquid phase compositions of this plot indicate the AR (Equation 6).

$$x_{P,AR} = \frac{\dot{M}_{P,AR}}{\dot{M}_{P,AR} + \dot{M}_{W,AR}} \quad (6)$$

The AZ (secondary y-axis) of the 1-propanol/water mixture at 25 °C is at a composition of $x_{P,AZ} = 66.5$ wt%. With similar assumptions, the AR in dry air (primary y-axis) is at a composition of $x_{P,AR} = 53.3$ wt%. For $x_P < x_{P,AR}$, 1-propanol evaporates preferentially into the gas phase and water accumulates relatively in the remaining liquid phase. At higher 1-propanol concentrations ($x_P > x_{P,AR}$), the opposite effect can be observed and water evaporates preferentially from the liquid phase. Thus, if considering the gas kinetics with dry air, the range of preferred 1-propanol evaporation becomes smaller and the point identical liquid and gas-phase composition is at lower 1-propanol

compositions. This is attributed to the different mass transport kinetics of the components.

Experimental studies by Koga et al.^[6] and Scheepers et al.^[10,11] have experimentally demonstrated these changes in ink composition during ink drying for fuel cells. However, a theoretical model for predicting the drying behavior of catalyst inks remains to be developed and evaluated. This is the focus in this study.

2.1. Influence of the Drying Parameters on the Arheotropic Compositions of a Binary 1-Propanol/Water Mixture

Incorporating the gas-phase kinetics into the analysis of the mixture evaporation allows for a more accurate description of a ink drying process considering selective evaporation. To investigate the influence of key drying parameters on the AR, a series of parametric studies are conducted, focusing on the effects of drying temperature, air overflow (in the form of the heat transfer coefficient for describing the convective flow independent of dryer geometries), and air pre-loading in form of relative humidity. **Figure 2** shows the relative evaporation rate of 1-propanol over the propanol composition (x_P) as a function of different (film) temperatures (a) and heat transfer coefficients (b). The air is assumed to be completely dry, with no pre-loading of water (relative humidity) or 1-propanol.

The investigated temperatures correspond to those of the liquid phase, as the underlying mass and energy balances are formulated with respect to this phase. In the convective evaporation processes, the temperature of the liquid is substantially lower than that of the air flow due to the evaporative cooling. Depending on the composition of the liquid phase, film temperatures in the range of 10–40 °C correspond to air temperatures between 17 °C and 170 °C.

As the temperature increases, the arheotropic composition shifts toward higher 1-propanol concentrations. This leads to

an expanded range of composition for preferential evaporation of 1-propanol. While at a temperature of 10 °C the AR is 51.3 wt%, at 40 °C it is $x_{P,AR,40\text{ °C}} = 55.0$ wt%. An increase in film temperature of 30 °C therefore results in a shift in $x_{P,AR}$ of only 3.7 wt%. This shift occurs, because the vapor pressure of 1-propanol increases slightly more than that of water with rising temperature.

Furthermore, when analyzing the shift of $x_{P,AR}$ at intervals of 10 °C, it is noticeable that the distance between successive arheotropic points diminishes at higher temperatures.

The heat transfer coefficient does not influence the position of the arheotropic point, which remains constant at $x_{P,AR} = 53.3$ wt% at a temperature of 25 °C and dry air. This can be explained by the fact that the gas-phase kinetics separation factor, according to Riede and Schlönder,^[16] only changes by 0.3% within the examined range of mass flow rates. The low heat transfer coefficient of 5 W/(m² K) is analogous to free convection. As a result, evaporation governed purely by thermodynamic control can only occur under idealized conditions, such as in a saturator, and not in the actual drying process of catalyst layers. Consequently, the influence of the heat transfer coefficient, or alternatively the air flow rate, is neglectable within the scope of the investigated parameters.

However, increasing drying temperature or heat transfer coefficient may not significantly influence selectivity but accelerate the drying itself.

The final drying parameter investigated is the pre-loading of the drying air with an ink solvent. The pre-loading of the drying air, for example with water (humidity), has a significant impact on the evaporation behavior of the solvent mixture comprising 1-propanol and water. This is demonstrated in **Figure 3**, which illustrates the effect of increasing humidity, from dry air to air completely saturated with water, on the position of the AR. The film temperature is set to 25 °C.

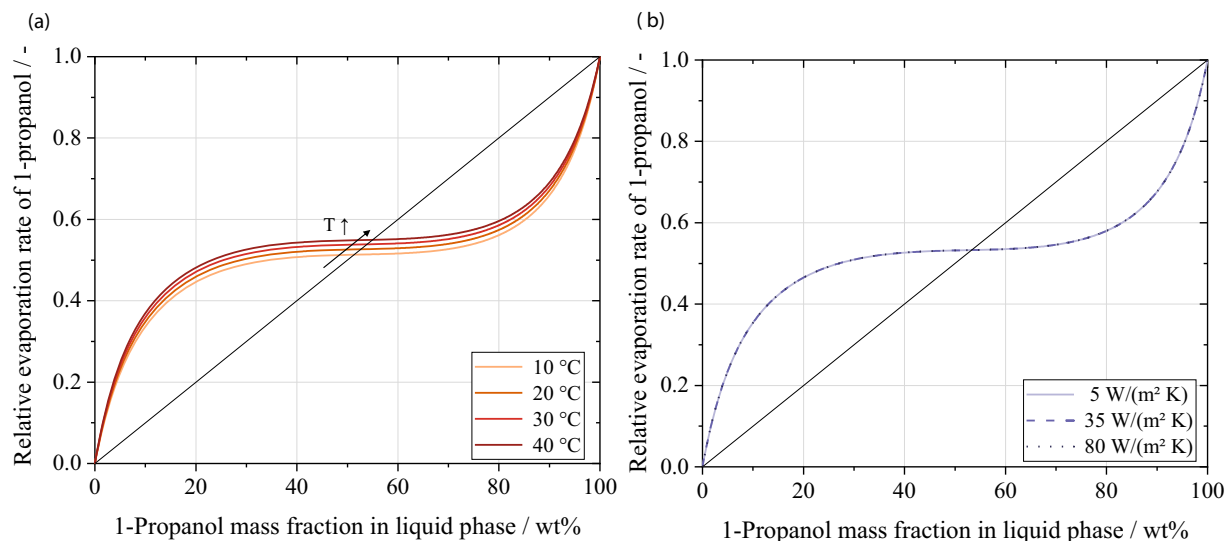


Figure 2. Relative gravimetric evaporation rate of 1-propanol as a function of liquid composition of a binary 1-propanol/water solvent mixture (1-propanol (P) mass fraction x_P) at 25 °C and without air pre-loading: a) is showing the influence of (film) temperature and b) neglectable impact of the heat transfer coefficient (linked to the air flow rate) on the position of the arheotropic point (intersection with the angle bisecting). For compositions lower than the arheotropic composition, 1-propanol evaporates preferential. Both individual drying parameters only have a minor influence on the arheotropic point.

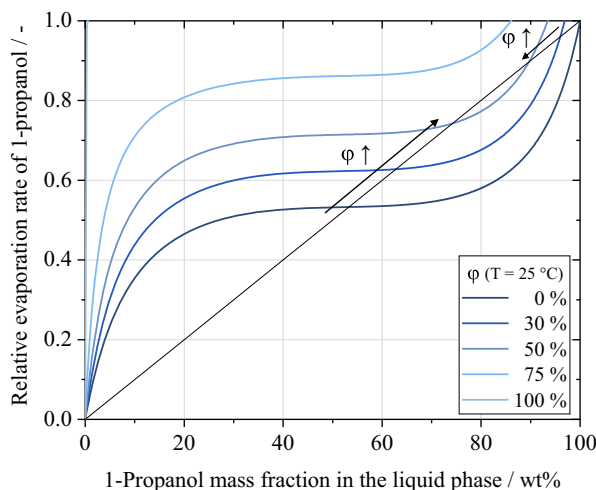


Figure 3. Relative gravimetric evaporation rate of 1-propanol as a function of the liquid composition of a binary 1-propanol/water solvent mixture (1-propanol (P) mass fraction x_P) at 25 °C. The influence of air pre-loading with water (relative humidity, ϕ) on the arheotropic compositions (intersection with the bisector) is shown. The range of compositions in which water evaporates preferentially ($x_{P,AR} > x_P > x_{P,AR}^*$) is either reduced or absent as a consequence of the pre-loading of the drying air.

As relative humidity increases, the evaporation kinetics of water is hindered. In consequence, the arheotropic point shifts toward higher 1-propanol concentrations, expanding the range where $x_P < x_{P,AR}$ and preferential 1-propanol evaporation. Due to the relative humidity, there is a second intersection of the curve with the bisector at higher 1-propanol contents and thus a second arheotropic point ($x_{P,AR}^*$). The second arheotropic point further reduces the area in which water evaporates preferentially. For mixture concentrations of $x_{P,AR} < x_P < x_{P,AR}^*$, water evaporation is favored. The AR for the relevant analyzed humidity levels are presented in Table 1. At a certain critical humidity level, there is no longer an intersection with the bisector, indicating that preferential evaporation of water is no longer possible. 1-propanol will continue to evaporate preferentially with any solvent mixture composition.^[17]

This analysis is particularly relevant for fuel cell processing in environments without preconditioned drying air or drying ovens. In such conditions, humidity levels can vary considerably based on climatic, seasonal, and geographical factors. For instance, in Karlsruhe, Germany, humidity fluctuations in a range of 15–75% (at 25 °C) occur between summer and winter, influencing the solvent's evaporation behavior and thereby affecting the film composition during drying. Changes in solvent composition can also

Table 1. 1-Propanol compositions for the first ($x_{P,AR}$) and second ($x_{P,AR}^*$) arheotropic point at increasing relative humidity (ϕ) of the drying air at 25 °C.

ϕ (T = 25 °C)	$x_{P,AR}$	$x_{P,AR}^*$
0%	53.5%	—
30%	62.7%	96.0%
50%	74.2%	89.7%

influence particle–particle or ionomer–particle interactions, as well as important ink properties, such as surface tension and mixture density.^[4,7,10,24–26] This is further explored in chapter 2.2 and 2.3.

Pre-loading the air with 1-propanol or with both solvents, as may occur in the air circulation mode of a convection dryer, further influences the arheotropic point.

To summarize, it is essential to specify the pre-loading of the drying air (indicated by the dew point or relative humidity and temperature) as an important factor in drying of catalyst layers. This is necessary in order to enable the comparison of results from different studies. Furthermore, on an industrial scale, conditioning of the air to achieve constant pre-loading should be taken into consideration.

2.2. Influence of Varying Relative Humidity on the Drying of Catalyst Inks

The following section combines the purely theoretical consideration of selectivity with the drying of catalyst inks. The aim is to compare the effect of air pre-loading in a realistic drying process for fuel cells and electrolyzers. For this purpose, a catalyst layer with an area of $9 \times 9 \text{ cm}^2$ and an initial composition of $x_{P,0} = 53 \text{ wt\%}$ 1-propanol, $x_{W,0} = 36 \text{ wt\%}$ water and $\omega_{\text{solids},0} = 11 \text{ wt\%}$ solid components (equivalent to a pure solvent composition of 60 wt% 1-propanol and 40 wt% water) is assumed, which undergoes convective drying at an air temperature of 72 °C and a heat transfer coefficient of $35 \text{ W/(m}^2 \text{ K)}$. Under these applied drying conditions, and considering the ink formulations and selective solvent evaporation behavior, the calculated film temperature is 25 °C in the examined first drying period. The porosity of the dried electrode is set to $\varepsilon = 65\%$ for the calculation of the end-of-film shrinkage (EOFS) (Equation (1)). These conditions (Table 2) are held constant to isolate the effect of water pre-loading of the air on the drying process.

Table 2. Drying and ink parameters for the simulation of the selectivity of drying of a binary 1-propanol/water mixture in catalyst inks. First, the only difference in the simulation parameters is given by air pre-loading, which is increased from 0.0 % ($\bar{y}_{W,\infty} = 0.000$) to 28.5 % (at 25 °C, $\bar{y}_{W,\infty} = 0.009$, $\tau = 5.5 \text{ s}$). Later, the influence of solvent composition is investigated by reducing the initial 1-propanol content from 53 wt% to 18 wt%.

Symbol	Without air pre-loading	With air pre-loading
$\bar{y}_{W,\infty}$	0.000	0.009
$\bar{y}_{P,\infty}$	0.000	
T_{conv}	72 °C	
α	$35 \text{ W/(m}^2 \text{ K)}$	
A_{Ph}	0.0081 m^2	
$x_{P,0}$	53 wt%	
$x_{\text{solid},0}$	11 wt%	
ε	65 %	
x_{EOFS}	37.5 wt%	

Film-side mass transport resistances are neglected in this study. Consequently, the analysis is only conducted up to the calculated EOFS. It is similarly anticipated that the EOFS will correspond with the beginning of crack formation in the layers. Given the influence of a changing ink composition on the interaction of the ionomer and catalyst particles and thus the microstructure formation (e.g., cracking), this model is expected to be important to further examine cracking during electrode drying.

Figure 4 shows the composition of the catalyst layer against the normalized drying time (t/t_{end}) for different air pre-loadings with water. The colors in both diagrams and the pie charts (representing the start of drying and EOFS) correspond to the proportions of solids (gray or white), water (blue), and 1-propanol (red) during the drying process. The solid line indicates the total solvent content in the ink during drying. To elaborate the influence of varying ink composition during drying, schematic illustrations based on the findings from Ngo et al.^[7] and Mabuchi et al.^[40] are presented above the corresponding diagrams. These schematics show the composition-depended changes of Nafion morphology (turquoise) and the interactions between Nafion and the catalyst particles (black) during the drying process, which may effect microstructure formation.

Both drying curves start with a solvent content of 89 wt%. Before beginning the drying process, the catalyst ink consists of 11 wt% solids (catalyst and ionomer), 53 wt% 1-propanol, and 36 wt% water (initial 1-propanol to water mass ratio 60:40). In the case of drying with dry air (a), the solvent composition shows that 1-propanol progressively accumulates relatively as the overall solvent content decreases. As the drying process continues, the water content of the film decreases. By the EOFS, the ink is composed almost entirely of 1-propanol and

solids. This occurs because the initial solvent composition is greater than the azeotropic composition of the 1-propanol/water mixture in dry air ($x_{\text{P},0} = 60 \text{ wt\%} > x_{\text{P},\text{AR}} = 53.3 \text{ wt\%}$).

In contrast, during the drying of the ink with pre-loaded air ($\bar{y}_{\text{w},\infty} = 0.009$, dew point: $\tau = 5.5^\circ\text{C}$), the evaporation kinetics of water is inhibited. With gas-phase kinetics considered, the solvent composition is now below the azeotropic point ($x_{\text{P},0} = 60 \text{ wt\%} < x_{\text{P},\text{AR},\tau=5.5^\circ\text{C}} = 62.7 \text{ wt\%}$), resulting in the preferential evaporation of 1-propanol. Consequently, water accumulates relatively in the remaining solvent mixture. Despite starting with the same initial composition, at the EOFS only 27 wt% water and 8 wt% 1-propanol remain in the catalyst film. The humidity of the air also extends the drying time, in this specific case by 5.6%.

The effect of the significantly different composition profiles over the drying time is likely to be further intensified by higher air pre-loadings. Also, an impact of these composition changes on the self-interactions of Nafion and interactions between the ionomer and the catalyst particles is anticipated. According to Ngo et al.^[7] with the initial catalyst ink composition, Nafion exists predominantly as aggregated, rod-like structures with a strong negative charge. This morphology can impede deposition onto the catalyst particle surfaces. During the drying process, if 1-propanol accumulates in the ink (Figure 4a), Nafion undergoes a morphological transition to smaller, more flexible aggregates with a reduced surface charge. The attachment to the catalyst surface is facilitated. In contrast, the preferential accumulation of water (Figure 4b) promotes the formation of larger, highly agglomerated Nafion structures that maintain a strong negative charge, further inhibiting their interaction with the catalyst particles. These morphological and interactional changes

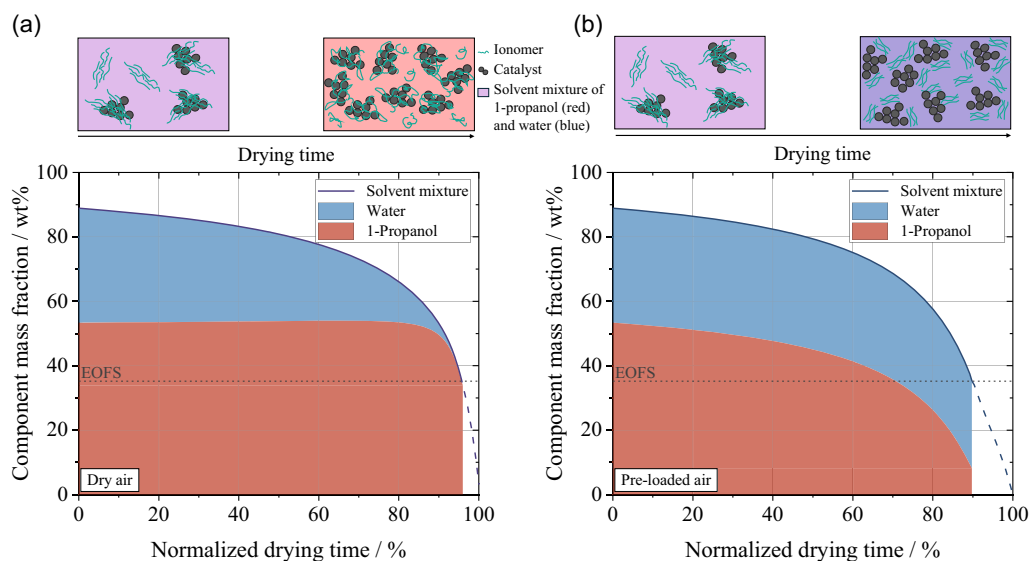


Figure 4. Simulation of the ink composition in the first drying period (until EOFS) of a catalyst ink composing of a 1-propanol water mixture over the normalized drying time t/t_{end} without a) and with b) air pre-loading ($\bar{y}_{\text{w},\infty} = 0$ and $\bar{y}_{\text{w},\infty} = 0.009$) and 72°C . The ink composition is symbolized by colors (red: 1-propanol, blue: water, gray and white: solids). With pre-loading of the air, the selectivity of the drying (preferable evaporation of one component) is inverted. An air pre-loading with water hinders the water evaporation and water is relatively enriched in the ink. Adapted from the work of Ngo et al.^[7] and Mabuchi et al.,^[40] the schematic illustrations above the diagrams show the changes in interactions between the Nafion ionomer (turquoise) and the catalyst particles (black) at different solvent compositions along the drying process, indicated by the background color coding (mixture of 1-propanol (red) and water (blue)).

significantly influence the resulting microstructure of the catalyst layer, including, for example, the mechanical resistance for cracking. Consequently, considerations on selective solvent evaporation and its effects on film formation must be integrated into the design of the drying process at both laboratory and production scale.

2.3. Influence of Varying Initial Ink Formation on the Drying of Catalyst Inks

Next, the impact of ink formulation under constant drying conditions on the solvent composition during drying is investigated. For this analysis, the simulation parameters established in the previous study, involving water pre-loading air with a dew point of $\tau = 5.5^\circ\text{C}$, are maintained (see Table 2). The focus is on comparing the drying behavior and solvent composition between two ink formulations: a) 11 wt% solids (catalyst and ionomer), 36 wt% water, and 53 wt% 1-propanol (identical to Figure 4), and b) 11 wt% solids, 71 wt% water, and 18 wt% 1-propanol. Figure 5 illustrates the simulated drying curves for both ink compositions.

Based on the initial solvent composition ($x_{P,0} < x_{P,AR}$) at the given temperature and pre-loading of the drying air, an accumulation of water is expected for both formulations. For the ink with $x_{P,0} = 53\text{ wt\%}$, the evaporation is observed to be only slightly selective. At the EOFs, the mass fraction of 1-propanol is reduced to 8 wt%. The drying layer at this stage consists of 27 wt% water and 65 wt% solids, alongside the residual 1-propanol.

The schematic illustrations above the diagrams depict how these changes in ink composition influence the morphology and interactions of Nafion in the catalyst ink.

In contrast, the second ink formulation (b), characterized by a higher initial water content ($x_{W,0} = 71\text{ wt\%}$ and $x_{P,0} = 18\text{ wt\%}$), shows rapid 1-propanol depletion due to its preferred evaporation. By 44% of the total drying time, nearly all 1-propanol has evaporated ($x_P < 1.0\text{ wt\%}$), leaving water as the predominant evaporating solvent. The drying rate is subsequently reduced due to the slower evaporation kinetics of pure water in comparison to the solvent mixture. Consequently, the drying time for this formulation is extended by 50.6% compared to the ink with $x_{P,0} = 53\text{ wt\%}$. With respect to the interactions between the solid components (Nafion and catalyst particles) within the ink, the accumulation of water in both ink formulations at the applied drying conditions promotes the formation of larger, highly negatively charged Nafion agglomerates. The deposition of these structures to the catalyst surface is hindered. For the ink with $x_{P,0} = 18\text{ wt\%}$ (Figure 5b), water is almost exclusively present throughout most of the drying process. Consequently, pronounced changes in the ionomer–catalyst interactions are expected.

These variations in initial solvent composition and the evolving solvent distributions during drying have a great influence on the (self)interactions of the ionomer and the catalyst particles. The influence of different initial solvent mixtures in catalyst inks on electrode properties has been demonstrated in several studies.^[24,40] Nevertheless, the effect of varying solvent composition during drying on electrode properties remains to be explored in future investigations. For instance, targeted adjustments to the air pre-loading could be used to manipulate the composition profile during the drying process, offering potential for fine-tuning electrode properties.

In the present study, solely solvent mixtures of 1-propanol and water are investigated as this solvent system is widely used for

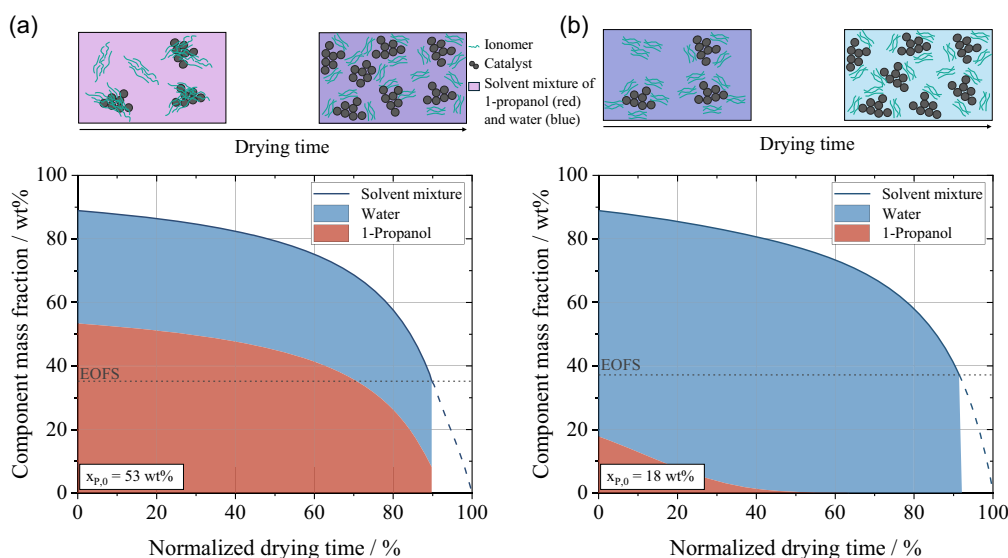


Figure 5. Simulation of the ink composition in the first drying period (until EOFs) with constant drying conditions ($T_{\text{conv}} = 72^\circ\text{C}$, $\bar{y}_{w,\infty} = 0.009$) for different initial solvent compositions ($x_{P,0} = 53\text{ wt\%}$ and $x_{P,0} = 18\text{ wt\%}$). The ink composition is symbolized by colors (red: 1-propanol, blue: water, gray: solids). While for $x_{P,0} = 53\text{ wt\%}$ a) both solvents are present in the drying ink during the entire drying process, for $x_{P,0} = 18\text{ wt\%}$ b) mainly water, is present in the ink for the majority of the drying time. Adapted from the work of Ngo et al.^[7] and Mabuchi et al.,^[40] the schematic illustrations above the diagrams show the changes in interactions between the Nafion ionomer (turquoise) and the catalyst particles (black) with different solvent compositions along the drying process, indicated by the background color coding (mixture of 1-propanol (red) and water (blue)).

fuel cell catalyst inks.^[9,11,23–25,41,42] However, future work will aim to systematically expand the analysis to include a broader range of solvent systems.

3. Evaluation of the Theoretical Model with Experimental Results of a Drying Catalyst Layer

To evaluate whether the theoretical model can be used to describe experimental data for catalyst layers for PEM fuel cells or electrolyzers with a binary 1-propanol/water mixture, the drying behavior of catalyst inks is now being investigated.

The catalyst ink is prepared using a CN10 dissolver with an APS250 bead mill attachment (VMA Getzmann GmbH, Germany). The ink formulation consisted of catalyst particles (TEC10EA50E, Tanaka Kikinzoku, Japan), Nafion dispersion (D2020, IonPower, USA), and a solvent mixture of 1-propanol (Carl Roth, Germany, purity > 99.5%) and water (ultrapure). The ink was processed for 3 h at 1000 rpm. Beads of Yttrium-stabilized zirconium oxide (0.6–0.8 mm) were used in the ball mill, with a bead-to-ink volumetric ratio of 1:1.

For the investigation of gravimetric drying behavior, the ink was applied to a polytetrafluoroethylene (PTFE) substrate (Hightechflon, Germany) using doctor blade coating (ZUA200, Zehntner, Switzerland) and dried under controlled conditions using a Comb Nozzledryer (CN Drying Technology, Germany). The drying setup is characterized by a homogeneous nozzle field equipped with integrated exhaust air extraction, ensuring uniform drying conditions. The drying air is not preconditioned with respect to humidity prior to entering the dryer; rather, the drying air is heated ambient air. During experiments, the relative humidity is closely monitored to ensure reproducibility of test conditions. The continuous monitoring of ambient parameters allows their direct use as input variables for the simulation model.

The electrodes were placed on a precision balance (MC1 LC 1200 S, Sartorius, Germany) during the drying process to record their gravimetric drying curves. The ink formulation, coating parameters (dry film thickness $9.6 \pm 1.0 \mu\text{m}$), and drying conditions (air temperature $T_{\text{conv}} = 72^\circ\text{C}$, heat transfer coefficient $\alpha = 35 \text{ W}/(\text{m}^2 \text{ K})$, humidity of the drying air $\tilde{y}_{\text{w},\infty} = 0.009$, honeycomb nozzle field) were kept constant throughout the experiments. More detailed information on the experimental setup can be found in.^[43] **Figure 6** shows the evaluation of the theoretical model with experimental data of the drying of catalyst inks with the initial compositions of $x_{\text{p},0} = 53 \text{ wt\%}$ and $x_{\text{p},0} = 18 \text{ wt\%}$ at the specified drying conditions. For validation, gravimetric drying curves from three independent experiments (Figure 6a, b) conducted under identical drying conditions are presented (with filled, half-filled, and unfilled data points). The observed deviations between data points arise primarily from the limitations of the experimental setup—namely, the use of a high precision balance in combination with the convective heat input—and minor variations in ink application. For reference, the drying behavior assuming non-selective evaporation is also presented (dashed line). Despite the signal-to-noise ratio, the experimental results remain sufficient to demonstrate the significance of incorporating selective evaporation into the simulation model. To provide deeper insight into the solvent composition within the ink,

Figure 6 c, d also presents the compositions along the drying process obtained with the simulation with selective evaporation.

The simulative description of the drying process based on selective solvent mixture evaporation (solid line) provides an adequate representation of the experimental drying behavior (data points) for both catalyst inks. Notably, only the selective simulation successfully captures the markedly different drying dynamics and durations observed under identical drying conditions for both inks. However, for solvent compositions near the azeotropic point (Figure 6a), both simulation approaches (with and without consideration of selective evaporation) yield similar drying predictions. At the applied drying conditions and with the ink formulation, the solvent composition does not change significantly, allowing the non-selective evaporation model to describe the drying process. In contrast, for the ink formulation with a substantially lower initial solvent composition than the azeotropic composition (Figure 6b), the drying time is underestimated by the non-selective model due to the unaffected evaporation of both solvents. A detailed evaluation of the simulation results for selective and non-selective evaporation can be found in the Supporting Information S1. Additional supporting measurements with comparative analyses between experimental data and simulation results for both ink formulations at an alternative drying temperature, are provided in supporting information S2.

With regard to the ink composition during drying (Figure 6c,d), in the ink with an initial 1-propanol content of $x_{\text{p},0} = 53 \text{ wt\%}$, both solvents remain present throughout the first drying period (up to the EOFs). In contrast, the simulation for the ink with $x_{\text{p},0} = 18 \text{ wt\%}$ indicates that after 38 s the 1-propanol content has fallen below 1 wt%. The solvent compositions at EOFs for both inks are provided in **Table 3**.

When comparing the drying behavior in the first drying period of the two inks with different initial solvent compositions, it is noticeable that the drying of the ink with $x_{\text{p},0} = 53 \text{ wt\%}$ is about 54% faster than the ink with $x_{\text{p},0} = 18 \text{ wt\%}$ at similar drying conditions. The observed differences in drying time can be explained with the evaporation kinetics and thermodynamics of the mixture, which is influenced by the activity, the partial pressures, and diffusion coefficients of the components in the mixture. Also considering the specific evaporation enthalpy of the components (1-propanol: $\Delta h_{\text{v,p}} (T = 25^\circ\text{C}) = 802 \text{ kJ kg}^{-1}$ and water: $\Delta h_{\text{v,w}} (T = 25^\circ\text{C}) = 2441 \text{ kJ kg}^{-1}$ ^[37]) and the evaporation kinetics lead to different wet bulb temperatures for the mixtures depending on their composition during the first drying period (25°C for $x_{\text{p},0} = 53 \text{ wt\%}$ and 27°C for $x_{\text{p},0} = 18 \text{ wt\%}$, respectively). Combining these factors results in a lower drying rate and higher wet bulb temperatures for the ink with $x_{\text{p},0} = 18 \text{ wt\%}$ compared to the ink with $x_{\text{p},0} = 53 \text{ wt\%}$ at identical drying conditions.

Additionally, the composition of the ink–solvent mixture changes significantly throughout the drying process. For the ink with $x_{\text{p},0} = 53 \text{ wt\%}$, both solvents remain present throughout the entire first drying period. In contrast, the ink with a lower initial 1-propanol content ($x_{\text{p},0} = 18 \text{ wt\%}$) predominantly contains water from approximately halfway through the drying process according to the simulation. As the composition of the dispersing medium affects the interactions between ionomer and catalyst and the capillary pressure, these concentration variations can significantly influence the electrode (micro) structure, including the formation of cracks.^[4,10,23,25]

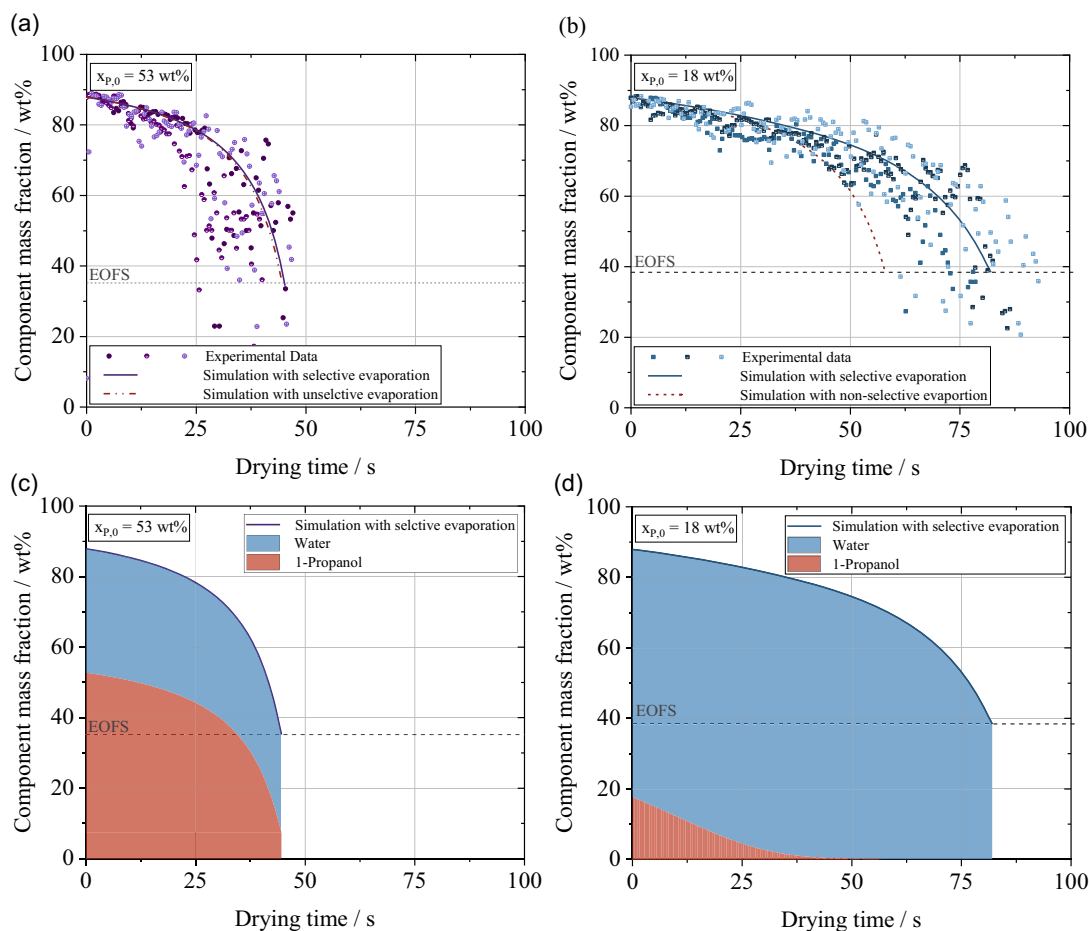


Figure 6. Comparison of the experimentally detected drying behavior (data points from three experiments) of two catalyst inks with a) $x_{p,0} = 53\text{ wt}\%$ (purple) and b) $x_{p,0} = 18\text{ wt}\%$ (blue) with the simulation of the solvent mixture evaporation during the first drying period (solid line). The drying conditions were kept constant at $T_{\text{conv}} = 72^\circ\text{C}$ (corresponding to an experimentally recorded average film temperature of 25°C (left) and 27°C (right)), $\bar{y}_{w,\infty} = 0.009$ and $\alpha = 35\text{ W}/(\text{m}^2\text{ K})$ for both the simulations and the experiments. The solid line represents the simulation results based on a drying model incorporating selective evaporation, whereas the dashed line corresponds to a model assuming non-selective evaporation. The drying behavior of both inks can only be accurately described by the selective evaporation model, particularly when the initial solvent composition deviates significantly from the azeotropic composition (b,d). In such cases, substantial compositional changes occur during drying, which are not adequately represented by the non-selective model. The diagrams c,d) illustrate the ink composition during selective evaporation, represented by color coding (red: 1-propanol, blue: water). Changing solvent compositions, which influence the drying behavior of the ink, can be observed as drying progresses.

Table 3. Calculated composition and drying time at the end-of-film shrinkage (EOFS) for the two inks studied, with an initial 1-propanol content of $x_{p,0} = 53\text{ wt}\%$ and $x_{p,0} = 18\text{ wt}\%$. Constant drying conditions ($T_{\text{conv}} = 72^\circ\text{C}$, $\bar{y}_{w,\infty} = 0.009$ and $\alpha = 35\text{ W}/(\text{m}^2\text{ K})$) were applied. Due to the different (initial) compositions, the drying time for the ink with $x_{p,0} = 18\text{ wt}\%$ is nearly twice as long.

At EOFS	Ink $x_{p,0} = 53\text{ wt}\%$	Ink $x_{p,0} = 18\text{ wt}\%$
$x_{\text{solid}}/\text{wt}\%$	64.8	62.8
$x_p/\text{wt}\%$	7.5	$2.4 \cdot 10^{-7}$
$x_w/\text{wt}\%$	27.7	37.2
t/s	44	82

Due to the experimental setup during the in-situ determination of the solvent decrease, the experimental data experience fluctuations. Until the EOFS, the mass change is sufficiently

large that it can be determined satisfactorily. For smaller mass changes (from EOFS) the signal-to-noise ratio becomes very small and the corresponding data has been excluded here for reasons of clarity.

Advancing from this, future investigations will focus on the formation of cracks during the drying of the catalyst layer, linked with the simulation of the selective drying process. This approach aims to provide a deeper understanding of crack formation mechanisms during drying to ultimately mitigate or control crack formation by adjusting drying parameters.

4. Conclusion

The theoretical analysis of the drying behavior of binary 1-propanol-water mixtures, commonly used in PEM fuel cells and electrolysis inks, highlights the significance of incorporating

gas-phase kinetics in evaporation behavior. The azeotropic point (thermodynamic + gas kinetics) can differ significantly from the azeotropic point (purely thermodynamic). A systematic evaluation of different drying parameters reveals that air pre-loading with water (relative humidity) shows the greatest influence on the azeotropic point. As humidity increases, the evaporation kinetics of water is impeded, resulting in a significant reduction in the composition range in which 1-propanol evaporates preferentially. At a critical humidity (depending on temperature), water evaporation is sufficiently hindered, resulting in a favored evaporation of 1-propanol across all mixture compositions.

Simulations investigating the impact of relative humidity on the first drying period of catalyst inks (neglecting material-side layer resistances) demonstrate that air pre-loading alone can reverse the drying selectivity. With dry air, 1-propanol tends to accumulate in a mixture with an initial composition of $x_{P,0} = 53$ wt%. However, when the relative humidity is raised to only 28% (at 25 °C), water starts to accumulate in the drying layer. These results show the importance of specifying air pre-loading as a critical drying parameter in both academic and industrial context to ensure reproducible drying conditions. Conditioning of the drying air is advised for industrial processes.

Furthermore, the initial solvent composition can lead to different solvent compositions during the drying process. Only a single solvent (e.g., water) may dominate for most of the drying process, impacting interactions within the ink matrix and ink properties and thus the electrode microstructure or crack formation.

The drying simulations were validated using experimentally determined gravimetric drying curves for catalyst layers. The results confirm that the drying behavior of these inks can be described sufficiently by only modeling the selective solvent evaporation.

Supporting Information

Supporting Information is available from the Wiley Online Library or from the author.

Acknowledgements

Open Access funding enabled and organized by Projekt DEAL.

Conflict of Interest

The authors declare no conflict of interest.

Author Contributions

Nadine Zimmerer: conceptualization (lead); data curation (lead); formal analysis (lead); investigation (lead); methodology (lead); software (lead); validation (lead); visualization (lead); writing—original draft (lead); writing—review & editing (lead). **Philipp Quarz:** data curation (supporting); methodology (supporting). **Ellen Terhorst:** software (equal). **Linus Janning:** methodology (supporting); writing—original draft (supporting). **Philip Scharfer:** supervision (supporting). **Wilhelm Schabel:** supervision (supporting).

Data Availability Statement

The data that support the findings of this study are available from the corresponding author upon reasonable request.

Declaration of Generative AI and AI-Assisted Technologies in the Writing Process

During the preparation of this work, the authors used DeepL (DeepL SE) and ChatGPT (Open AI) to improve readability and clarity. The authors reviewed and edited the content after usage and take full responsibility for the content of the publication.

Keywords

1-propanol/water, catalyst layer production, ink drying, PEM electrolysis, PEM fuel cells, selective evaporation, solvent composition

Received: March 17, 2025

Revised: May 14, 2025

Published online:

- [1] A. T. Mayyas, M. F. Ruth, B. S. Pivovarov, G. Bender, K. B. Wipke Manufacturing Cost Analysis for Proton Exchange Membrane Water Electrolyzers. Golden, CO: National Renewable Energy Laboratory. **2019**. <https://doi.org/10.2172/1557965>.
- [2] M. Kim, J.-N. Park, H. Kim, S. Song, W.-H. Lee, J. *Power Sources* **2006**, 163, 93.
- [3] T. Van Cleve, S. Khandavalli, A. Chowdhury, S. Medina, S. Pylypenko, M. Wang, K. L. More, N. Kariuki, D. J. Myers, A. Z. Weber, S. A. Mauger, M. Ulsh, K. C. Neyerlin, *ACS Appl. Mater. Interfaces* **2019**, 11, 46953.
- [4] H. Liu, L. Ney, N. Zamel, X. Li, *Appl. Sci.* **2022**, 12, 3776.
- [5] C.-H. Song, J.-S. Park, *Energies* **2019**, 12, 549.
- [6] M. Koga, H. Matsumoto, M. Tokita, H. Masunaga, T. Hikima, H. Sugimori, T. Sasabe, T. Yoshida, K. Shinohara, S. Hirai, *ECS Trans.* **2018**, 86, 157.
- [7] T. T. Ngo, T. L. Yu, H.-L. Lin, *J. Power Sources* **2013**, 225, 293.
- [8] P. Toudret, J.-F. Blachot, M. Heitzmann, P.-A. Jacques, *Catalysts* **2021**, 11, 669.
- [9] J. Park, Z. Kang, G. Bender, M. Ulsh, S. A. Mauger, *J. Power Sources* **2020**, 479, 228819.
- [10] F. Scheepers, A. Stähler, M. Stähler, M. Carmo, W. Lehnert, D. Stolten, *Coatings* **2018**, 8, 450.
- [11] F. Scheepers, A. Stähler, M. Stähler, M. Carmo, W. Lehnert, D. Stolten, *J. Coat. Technol. Res.* **2019**, 16, 1213.
- [12] S. Kundu, M. W. Fowler, L. C. Simon, S. Grot, *J. Power Sources* **2006**, 157, 650.
- [13] J. Zhao, X. Li, Z. Liu, *Int. J. Energy Res.* **2019**, 43, <https://doi.org/10.1002/er.4671>.
- [14] N. Kumano, K. Kudo, A. Suda, Y. Akimoto, M. Ishii, H. Nakamura, *J. Power Sources* **2019**, 419, 219.
- [15] N. Hasegawa, A. Kamiya, T. Matsunaga, N. Kitano, M. Harada, *Colloids Surf., A* **2021**, 628, 127153.
- [16] T. Riede, E. U. Schlünder, *Chem. Eng. amp; Technol.* **1988**, 11, 384.
- [17] P. Quarz, N. Zimmerer, P. Scharfer, W. Schabel, *Fuel Cells* **2024**, 24fuce.202300252 <https://doi.org/10.1002/fuce.202300252>.
- [18] M. B. Dixit, B. A. Harkey, F. Shen, K. B. Hatzell, *J. Electrochem. Soc.* **2018**, 165, F264.

- [19] E. Hoffmann, S. Zhang, M. Thoma, C. Damm, W. Peukert, *Particuology* **2019**, 44, 7.
- [20] J. Stoll, N. Zhao, X.-Z. Yuan, F. Girard, E. Kjeang, Z. Shi, *J. Power Sources* **2023**, 583, 233565.
- [21] Y. Komoda, K. Okabayashi, H. Nishimura, M. Hiromitsu, T. Oboshi, H. Usui, *J. Power Sources* **2009**, 193, 488.
- [22] S. Du, W. Li, H. Wu, P.-Y. Abel Chuang, M. Pan, P.-C. Sui, *Int. J. Hydrogen Energy* **2020**, 45, 29430.
- [23] T. Van Cleve, G. Wang, M. Mooney, C. F. Cetinbas, N. Kariuki, J. Park, A. Farghaly, D. Myers, K. C. Neyerlin, *J. Power Sources* **2021**, 482, 228889.
- [24] C. M. Baez-Cotto, J. R. Pfeilsticker, H. Yu, T. Van Cleve, B. T. De Villers, C. F. Cetinbas, N. N. Kariuki, J. H. Park, J. Young, D. J. Myers, D. A. Cullen, K. C. Neyerlin, M. Ulsh, S. Mauger, *J. Power Sources* **2024**, 592, 233852.
- [25] S. Takahashi, T. Mashio, N. Horibe, K. Akizuki, A. Ohma, *ChemElectroChem* **2015**, 2, 1560.
- [26] S. Holdcroft, *Chem. Mater.* **2014**, 26, 381.
- [27] A. F. Routh, *Rep. Prog. Phys.* **2013**, 76, 046603.
- [28] G. W. Scherer, *J. Am. Ceram. Soc.* **1990**, 73, 3.
- [29] J. Kumberg, M. Müller, R. Diehm, S. Spiegel, C. Wachsmann, W. Bauer, et al., *Energy Technol.* **2019**, 7, 1900722.
- [30] S. Jaiser, J. Kumberg, J. Klaver, J. L. Urai, W. Schabel, J. Schmatz, et al., *J. Power Sources* **2017**, 345, 97.
- [31] M. S. Tirumkudulu, W. B. Russel, *Langmuir* **2005**, 21, 4938.
- [32] K. B. Singh, M. S. Tirumkudulu, *Phys. Rev. Lett.* **2007**, 98, 218302.
- [33] D. Ramani, Y. Singh, F. P. Orfino, M. Dutta, E. Kjeang, *J. Electrochem. Soc.* **2018**, 165, F3200.
- [34] T. G. Tranter, M. Tam, J. T. Gostick, *Electroanalysis* **2019**, 31, 619.
- [35] C.-Y. Ahn, S. Jang, Y.-H. Cho, J. Choi, S. Kim, S. M. Kim, Y.-E. Sung, M. Choi, *Sci. Rep.* **2018**, 8, 1257.
- [36] E.-U. Schlünder, E. Tsotsas, *Wärmeübertragung in Festbetten, durchmischten Schüttgütern und Wirbelschichten: 33 Tabellen.*, Thieme, Stuttgart New York **1988**.
- [37] P. Stephan, S. Kabelac, M. Kind, H. Martin, D. Mewes, K. Schaber, *VDI-Wärmeatlas.*, Springer Berlin Heidelberg, Berlin, Heidelberg **2013** <https://doi.org/10.1007/978-3-642-19981-3>.
- [38] L. K. Jang, Y.-I. Chang, *Chem. Eng. Process Technol.* **2017**, 3(2): 1039.
- [39] E. N. Fuller, P. D. Schettler, *Ind. Eng. Chem.* **1966**, 58, 18.
- [40] T. Mabuchi, S.-F. Huang, T. Tokumasu, *Macromolecules* **2020**, 53, 3273.
- [41] S. Khandavalli, J. H. Park, N. N. Kariuki, D. J. Myers, J. J. Stickel, K. Hurst, K. C. Neyerlin, M. Ulsh, S. A. Mauger, *ACS Appl. Mater. Interfaces* **2018**, 10, 43610.
- [42] P. Quarz, N. Zimmerer, A.-M. Steck, P. Scharfer, W. Schabel, *Int. J. Hydrogen Energy* **2024**, 57, 789.
- [43] J. Kumberg, M. Baunach, J. C. Eser, A. Altvater, P. Scharfer, W. Schabel, *Energy Technol.* **2021**, 9, 2000889.